
This is an electronic reprint of the original article.
This reprint may differ from the original in pagination and typographic detail.

Freitas Vieira, Arthur; Vuckovac, Maja; Schlapp-Hackl, Inge; Hummel, Michael; Zhou, Quan
Droplet Probe for Characterization of Advancing and Receding Contact Angles of Single Fibers

Published in:

Proceedings of MARSS 2023 - 6th International Conference on Manipulation, Automation, and Robotics at Small Scales

DOI:

[10.1109/MARSS58567.2023.10294124](https://doi.org/10.1109/MARSS58567.2023.10294124)

Published: 01/01/2023

Document Version

Peer-reviewed accepted author manuscript, also known as Final accepted manuscript or Post-print

Published under the following license:

CC BY

Please cite the original version:

Freitas Vieira, A., Vuckovac, M., Schlapp-Hackl, I., Hummel, M., & Zhou, Q. (2023). Droplet Probe for Characterization of Advancing and Receding Contact Angles of Single Fibers. In S. Haliyo, M. Boudaoud, M. A. Qasaimeh, & S. Fatikow (Eds.), *Proceedings of MARSS 2023 - 6th International Conference on Manipulation, Automation, and Robotics at Small Scales* IEEE. <https://doi.org/10.1109/MARSS58567.2023.10294124>

This material is protected by copyright and other intellectual property rights, and duplication or sale of all or part of any of the repository collections is not permitted, except that material may be duplicated by you for your research use or educational purposes in electronic or print form. You must obtain permission for any other use. Electronic or print copies may not be offered, whether for sale or otherwise to anyone who is not an authorised user.

Droplet Probe for Characterization of Advancing and Receding Contact Angles of Single Fibers

Arthur Vieira, Maja Vuckovac, Inge Schlapp-Hackl, Michael Hummel, and Quan Zhou

Abstract— Characterizing the wetting properties of fibers is crucial for many research and industry applications, including textiles for water-oil separation and composite materials. Those fibers are often soft, typically tens of micrometers in diameter but millimeters in length, making manipulation and characterization difficult. Contact angles of single fibers are usually determined by droplet shape analysis or force-based Wilhelmy method. However, these methods are unable to accurately measure contact angles above 60° or ensure reliable control of the liquid-fiber interaction process, especially for soft fibers prone to bending. Consequently, reliable characterization of the advancing and receding contact angles of single fibers remains a challenge. Here we report a novel method for characterizing the advancing and receding contact angles of both soft and rigid single fibers using a millimeter-sized droplet probe affixed to a disk and a numerical model of the system. By analyzing side-view images, we extract key geometrical parameters of the disk-droplet-fiber system, which, when used in detailed simulations, allows estimating the contact angle of fibers ranging from 20° to 140° . We applied this method to characterize three distinct micro-fibers: a highly hydrophilic rigid borosilicate glass fiber, a mildly hydrophilic soft PET fiber, and a rigid hydrophobic tungsten wire coated with a commercial super-repellent coating.

I. INTRODUCTION

The characterization of wetting properties of surfaces and coatings has received significant interest in both industry and academia for its versatile applications, such as self-cleaning [1], fog-collection [2] and micro- and nano-assembly [3]. Of particular interest is the characterization of wetting properties of single fibers, which is becoming increasingly important for many fields requiring specific fiber wetting properties. For instance, in the fabrication of composite materials, high adhesion between the polymer matrix and the fiber mesh is crucial for achieving superior mechanical properties [4]. In water harvesting systems using fibers, low contact angle hysteresis allows droplets to readily move along the fiber to collection points [5]. In textiles for water-oil separation, selective wetting properties are crucial [6].

However, the characterization of wetting properties of single fibers is challenging due to experimental difficulties in manipulating micro-sized fibers [7] and measuring droplet-fiber interactions [8], [9]. Fibers used in textile fabrics and composite materials have diameters typically between 10 and $100\ \mu\text{m}$ and may be soft or fragile, making their manipulation difficult. Moreover, the shape of a droplet on a fiber is not spherical as it is on flat surfaces, and the cylindrical shape of the fiber greatly affects the droplet geometry. For hydrophilic fibers, the shape of the droplet is typically axisymmetric, for

which analytical solutions are available [10], [11]. This allows direct observation methods to be used, such as side-view contact angle goniometry, where geometrical parameters of the droplet can be directly related to the contact angle. However, the measurable contact angle range is limited to $0 - 60^\circ$ [10]. On more repellent fibers, the droplet takes an asymmetric configuration, i.e., the droplet partially wets the fiber taking a shape that resembles a clamshell [12], [13]. For super-repellent fibers, however, the droplet detaches from the fiber due to gravity or other disturbances, in which case direct observation of the contact angle is not possible.

Indirect techniques that can measure the contact angles of single fibers are difficult to apply on soft fibers or cannot reliably quantify advancing and receding contact angles. The modified Wilhelmy method is perhaps the most widely used and successful technique for the indirect measurement of advancing and receding contact angles of single fibers [8], [14]. The method consists of attaching one end of the fiber to a high-sensitivity force sensor, then submerging the other end in a test liquid. The measured force can then be analytically related to the contact angle, and advancing and receding contact angles can be measured during immersion and withdrawal of the fiber, respectively, using a motorized stage. However, this method is challenging to apply on soft fibers that tend to float or bend on the test liquid [15]. Also, the buoyant force may not be negligible for fibers with a diameter greater than $50\ \mu\text{m}$. Calibrated weights can be used to ensure the fiber is immersed and straight [16], which makes the estimation of buoyant forces less reliable. Moreover, the method requires a substantial amount of test liquid which must be free of contamination, often difficult to achieve in normal laboratory conditions.

Image-based contact angle goniometry is also used to measure the contact angle of single fibers, but the asymmetric clamshell configuration characteristic to contact angles above 60° , makes estimation of the water curvatures near the fiber difficult. One approach uses side-view imaging of the droplet along the axis of the fiber to obtain a clearer view of the contact angle [17], but the fiber must be rigid and supported from one side only. Another method uses two fibers to directly obtain contact angles from the geometrical parameters of a water droplet trapped between the fibers [18]. However, the fibers must have the same chemical and geometrical properties and be aligned parallel to each other. Magnetic fields are also commonly used to study droplet adhesion of fibers [19], where the probe liquid is required to be magnetic. Those magnetic methods generally focus on the detachment forces of droplets on fibers and are limited to mostly philic fibers.

Here we explore a method that uses a millimeter-sized droplet attached to a circular disk to characterize the advancing and receding contact angles of single fibers, which can be soft

Arthur Vieira and Quan Zhou are with the Department of Electrical Engineering and Automation, School of Electrical Engineering, Aalto University, 02150 Espoo, Finland (e-mails: arthur.vieira@aalto.fi; quan.zhou@aalto.fi).

Maja Vuckovac are with the Department of Applied Physics, School of Science, Aalto University, 02150 Espoo, Finland (e-mail: maja.vuckovac@aalto.fi)

Inge Schlapp-Hackl and Michael Hummel are with Department of Bioproducts and Biosystems, School of Chemical Engineering, Aalto University, FI-00076 Aalto, Finland

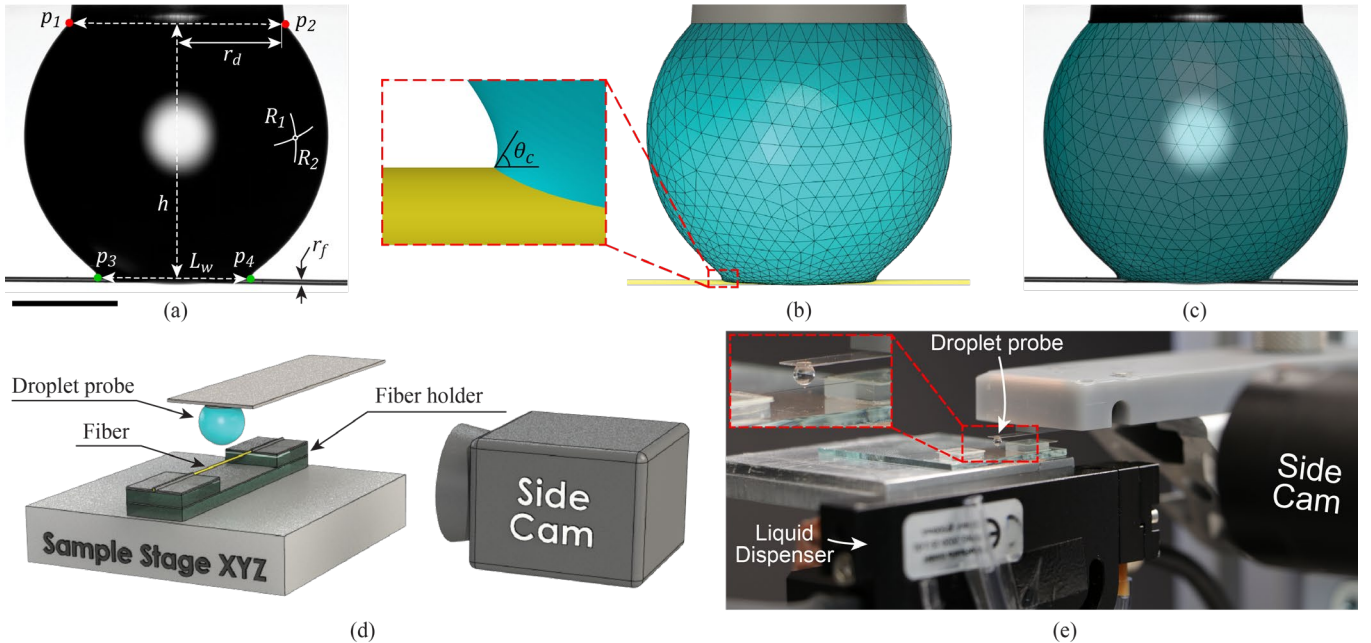


Figure 1 – Single fiber wetting characterization system. **(a)** Example of a side-view image of a droplet in contact with a fiber. The red dots, p_1 and p_2 , and green dots, p_3 and p_4 , illustrate key points obtained with machine vision identifying the position of the disk and the extremes of contact with the fiber, respectively. The wetting length L_w , disk-to-fiber height h , fiber radius r_f , and droplet volume V are also marked. (Scale bar: 500 μm) **(b)** Simulation result. Disk and fiber are rendered separately from the droplet simulation. The inset shows a close-up of the contact line region where the droplet outline meets the fiber. **(c)** Overlay of simulation result on the side-view image. **(d)** Illustration of the experimental setup (not to scale). A liquid droplet is held over a free-hanging fiber. A side-view camera images the shape of the droplet. A precision XYZ stage allows precise positioning of the fiber under the droplet **(e)** Experimental setup.

and phobic. The precise control of the droplet volume and location allows contact angles below and above 60° to be estimated numerically. The proposed disk-droplet-fiber system ensures the droplet is stable even when characterizing superhydrophobic or pre-tensioned soft fibers. By measuring key geometrical parameters obtained from the side-view analysis, we accurately simulate the droplet shape from which the contact angle can be estimated. We apply our method to three different fibers with contact angles ranging from 20° to 140° : a borosilicate glass fiber, a PET (Polyethylene terephthalate) fiber, and a tungsten wire coated with a commercial superhydrophobic coating.

II. CONCEPT

The wetting properties of surfaces are conventionally characterized by contact angle goniometry [20]. For a homogenous flat surface, a sessile droplet assumes the shape of a spherical cap, and the contact angle is measured by finding the intersection between a curve fitting the outline of the droplet and a baseline defining the plane between the sample and droplet. However, for a cylindrical surface such as single fibers, the droplet generally assumes a complex shape [13], as shown in Fig. 1a, making profile fitting challenging. Nonetheless, the equilibrium shape of the droplet can always be described by the Young-Laplace equation:

$$\frac{\Delta P}{\gamma} = \left(\frac{1}{R_1} + \frac{1}{R_2} \right), \quad (1)$$

where ΔP is the Laplace pressure, γ is the water-air surface tension, and R_1 and R_2 are the principal radii of curvature of the water-air interface at any point on the surface. The nonlinear partial differential equation can only be analytically solved for a few droplet-fiber systems, e.g., when the system has axial symmetry [8], occurring for fiber contact angles below 60° . Equation (1) also explains why curve fitting is challenging due to the droplet shape near the fiber, especially for thin fibers. In (1) $\Delta P/\gamma$ is constant while R_1 and R_2 vary at every point on the droplet surface. Near the fiber, Fig. 1b inset, the surface curvature of the droplet is $|R_2| \approx |R_1| \approx r_f$, where r_f is the radius of the fiber, and R_2 may have opposite sign of

R_1 . Far from the fiber, the radius of curvature is much bigger, $R_2 \approx R_1 \approx \sqrt[3]{V}$, where V is the volume of the droplet.

The shape of such asymmetric droplets can be solved by the method of energy minimization subject to constraints on the triple-phase contact lines, i.e., lines along which the liquid, vapor and solid phases meet, Fig. 1b and c. Our system uses a droplet-holding disk stabilizing the droplet, even if the fiber is water-repellent. At the top of the droplet, the triple-phase line is constrained to a circle with the same radius as the droplet-holding-disk, r_d . At the bottom, the shape of the triple-phase line, also known as the contact line (CL), is dependent on the contact angle of the fiber surface and the geometry of the fiber, which is taken as a cylinder with a known radius r_f .

In the disk-droplet-fiber system, we treat the contact angle of the fiber as an unknown function of key geometrical parameters of the droplet, shown in Fig. 1a.

$$\theta_c = f(L_w; h, V, r_f), \quad (2)$$

where, the wetting length L_w is the distance along the fiber wet by the droplet, h is the disk-to-fiber height, V is the volume of the droplet and r_f is the radius of the fiber. To measure the geometrical parameters L_w , h and V , we use machine vision to analyze the side-view image, through a combination of blob-analysis and geometric analysis discussed in section IV. The fiber radius r_f is measured with a microscope. These parameters are then used to simulate the shape of the droplet, shown in Fig. 2b. When θ_c is appropriately estimated the simulated droplet will match well the experimental observation, as shown in Fig. 2c.

III. APPARATUS

The key components used to characterize the contact angle of single fibers are shown in Fig. 1d and e. We use a droplet probe combined with precision motorized XYZ stages (models M-404.8PD, M-122.2DD and M-111.1DG, for the x, y, and z axes, respectively, from Physik Instrumente GmbH, Germany) and a side-view camera (camera: BFS-U3-28S5M C, Flir LLC; zoom-lens: VZM 600i, Edmund Optics Inc., USA). The probe consists of a millimeter-sized droplet attached to a disk underneath a glass-slide. The fiber is attached to a custom

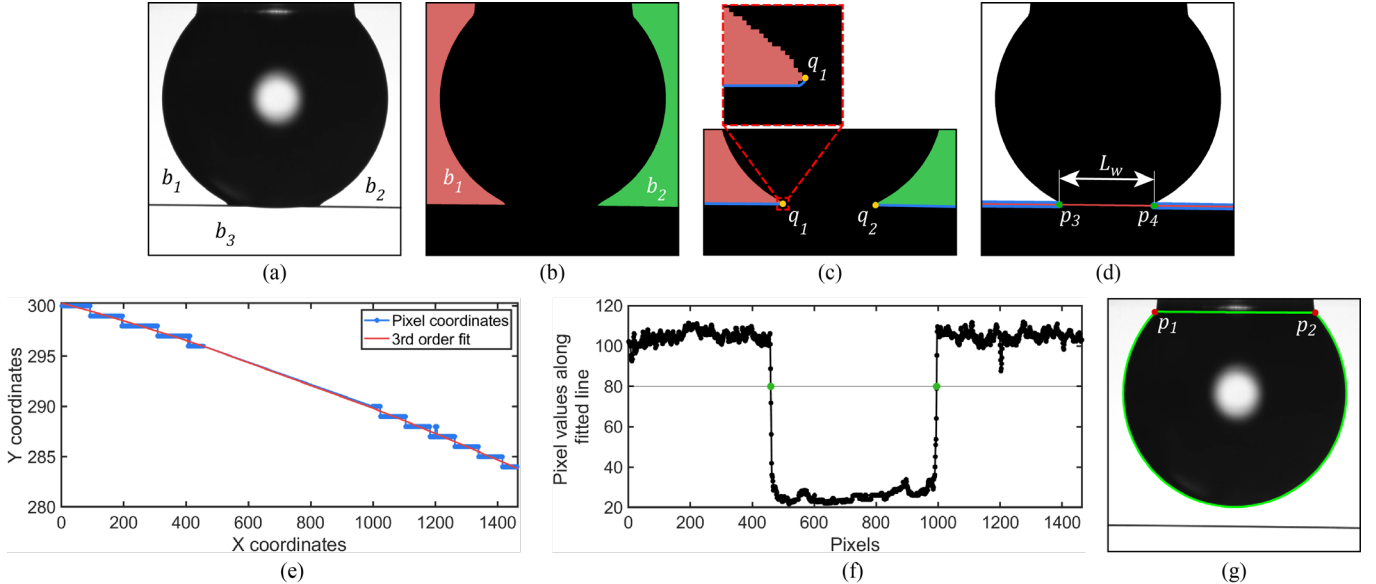


Figure 2 – Image analysis for determining the wetting length. **(a)** Raw side-view frame. **(b)** Binary threshold isolating the background to the left and right of the droplet. **(c)** The image is analyzed to find points q_1 and q_2 that define the line of the smallest droplet width (waist of the droplet). Inset shows close-up around q_1 where the droplet meets the fiber. **(d)** The top edge of the fiber (blue) on the left and right of points q_1 and q_2 , respectively, is fitted with a 3rd-order polynomial (red). **(e)** Plot of the top edge of the fiber (blue) and fitted curve (red). **(f)** The values of the pixels along the fitted line are obtained from the image. The points intersecting a setpoint value (black line) are shown in green. The distance between these two points in image space is considered the wetting length, as illustrated in **(d)**. **(g)** The volume is estimated from side-view images before and after the droplet is in contact with the fiber. Green outline represents the droplet edge detected with machine vision.

holder so that it is free-hanging across a gap of 10 to 20 mm. For the test liquid, we use a droplet of purified water (Direct-Q 3UV-R water purification system, Millipore SAS, France), formed on the underside of the disk with a non-contact-dispenser (PipeJet, BioFluidix GmbH, Germany). The dispenser is attached to the side of the motorized sample stage, where the geometrical configuration is measured and used in the measurement algorithm to achieve repeatable alignment beneath the droplet-holding disk. Before each experiment, the droplet is automatically refilled to a volume of $1.5 \mu\text{L}$, in line with similar studies [21], [22]. The respective droplet size ($\sim 1.44 \text{ mm}$) is well below the capillary length of water (2.7 mm), and the probe can capture the multi-scale wetting properties.

A typical characterization experiment starts by refilling the droplet and letting it evaporate until the target volume of $1.5 \mu\text{L}$ is reached. Then the fiber is moved underneath the droplet such that the top edge of the fiber is $20 \mu\text{m}$ away from the bottom edge of the droplet. The fiber starts moving upwards for $120 \mu\text{m}$ with a constant velocity of $10 \mu\text{m/s}$ and then moves downwards at the same speed until it detaches from the droplet. The whole characterization experiment is automated providing high repeatability and the interaction is recorded from the side-view camera at 100 fps.

IV. CONTACT ANGLE ESTIMATION METHOD

To obtain the geometrical parameters L_w and h , we analyze each side-view video frame with machine vision to find the two points defining the disk, p_1 and p_2 , and the two points defining the wetting interface p_3 and p_4 (shown in Fig 1a). The wetting length L_w is calculated as the distance between p_3 and p_4 , while the disk-to-fiber height is calculated as

$$h = |(p_2 + p_1)/2 - (p_4 + p_3)/2|. \quad (3)$$

The points p_1 and p_2 are found with template matching based on normalized cross-correlation [23], where the templates are manually selected from a reference image. The points p_3 and p_4 are found through the machine vision algorithm illustrated in Fig. 2. The raw frame is shown in Fig. 2a. We use a binary threshold to segment the three largest blobs in the image, the two background blobs on the sides of the droplet, b_1 , b_2 , and the blob underneath the droplet b_3

which is excluded from the analysis (Fig. 2b). Next, we focus the analysis on the bottom half of the image, where we find points q_1 , as the right-most pixel in the blob b_1 , and q_2 , as the left-most pixel in the blob b_2 (Fig. 2c). For contact angles below 90° , the edge of the droplet assumes a concave shape near the fiber, illustrated in the inset of Fig. 2c. For r_f much smaller than the droplet's half-width, q_1 and q_2 will be very close to the fiber but do not define well L_w . Instead, we take the coordinates of the edge pixels in b_1 along the fiber up to q_1 and the edge pixels in b_2 along the fiber up to q_2 (blue lines in Fig. 2c, d and e). These pixels are fitted with a 3rd-order polynomial (red line in Fig. 2d and e), which accounts for any fiber tilt or curvature resulting from fiber assembly. We then take the value of the pixels along the fitted line (black data points in Fig. 2f). The coordinate locations of p_3 and p_4 are found where the pixel values cross a specified threshold, e.g., 80 on a scale from 0 to 255.

The volume of the droplet at the frame of interest, V , cannot be directly measured from the side-view due to the asymmetric droplet shape. However, before and after contacting the fiber, the droplet has a spherical shape, which allows measuring the initial and final volumes from side-view images, V_i and V_f respectively. Fig. 2g shows the resulting analysis for estimating V_f from a side-view frame. First, we segment the droplet with a binary threshold (green outline in Fig. 2g). The points p_1 and p_2 are used to exclude the disk. Then, each cross-section is assumed to be circular and has a volume of $\pi r^2 \Delta p x$, where r is the half-width of the droplet at each row and $\Delta p x$ is the height of one pixel. The droplet volume is found by adding the volume of all rows. The volume at the keyframe, V , is then calculated by linear interpolation of V_i and V_f , based on the timestamps of their respective frames.

V. DROPLET SIMULATION

To find the shape of the droplet based on the geometrical parameters obtained from the side-view we use Surface Evolver (SE) [24]. SE is a finite element simulation tool for studying surfaces shaped by surface tension and other energies. The equilibrium surface shape is found by a gradient descent method, which finds the equilibrium droplet shape that minimizes the total energy of the system.

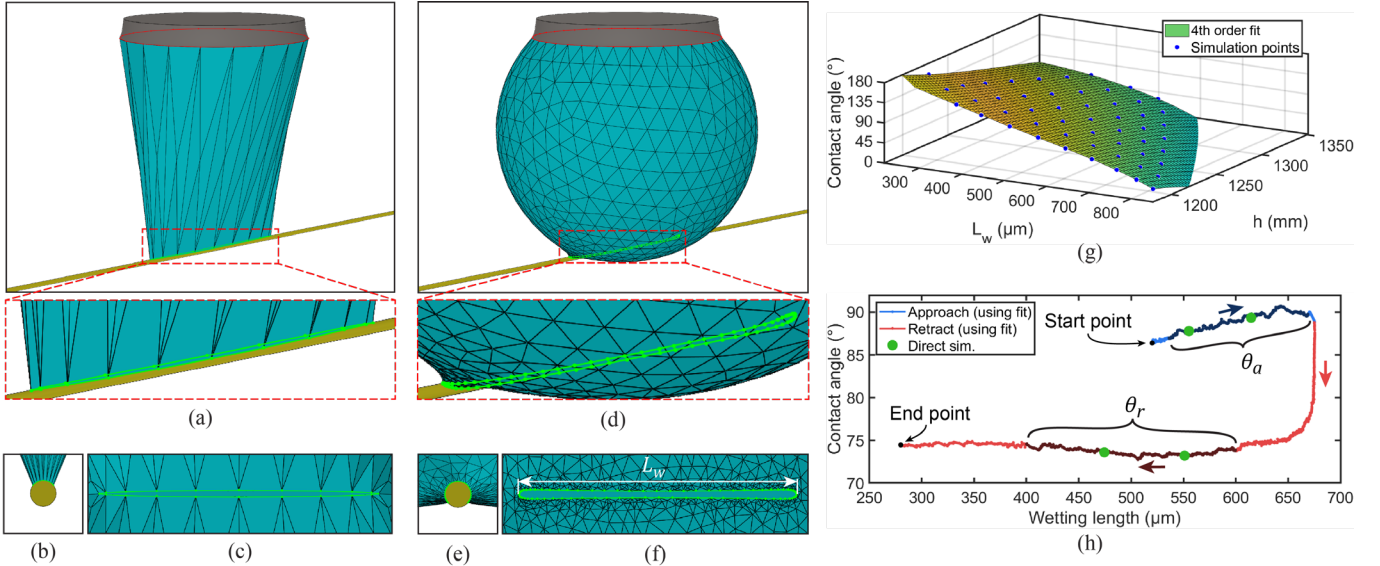


Figure 3 – Example simulation of a droplet in the disk-to-fiber system (parameters used: $r_f = 12.1 \mu\text{m}$, $V = 1.5 \mu\text{L}$, $h = 1207 \mu\text{m}$, $\theta_c = 62.3^\circ$). Disk (gray) and fiber (yellow) are rendered separately from simulation. (a) The initial state of the droplet. The inset shows a close-up of the CL (green). (b) Side-view close-up of the fiber region. (c) Bottom view of the CL (fiber not visible). (d) Final state of the simulation. The inset shows a close-up of the CL (green). (e) Side-view close-up of the fiber region. (f) Bottom view of CL (fiber not visible). (g) Plot showing the fitting of simulation data, $\theta_c(L_w, h)$. (h) Example curve for a complete approach-retract characterization experiment obtained using the fitted function. Shaded regions show where the mean advancing contact angle θ_a and mean receding angle θ_r are calculated. Green data points show the result of independent SE simulations, i.e., without fitted function.

Fig. 3 shows an example simulation. A disk-droplet-fiber simulation starts with an initial mesh surface (Fig. 3a-c) which does not yet satisfy either the volume constraint or energy minimum. At the top, the droplet is constrained to a disk with a radius of $r_d = 511 \mu\text{m}$, at a specified disk-to-fiber height h (red circle in Fig. 3a). At the interface with the fiber, the CL is constrained to an ellipse projected on the fiber of radius r_f . The CL is initialized to an ellipse projected on the fiber (green line in the inset of Fig. 3a and Fig. 3b-c), which is free to move during the energy minimization process. The droplet volume V and contact angle for the fiber surface, θ_c , are also specified. The latter defines the energy associated with the water-solid interface at the fiber, which is also subject to energy minimization during simulation.

The evolution of the droplet is a compromise between approximating the equilibrium shape and a practical computational time. The final shape is shown in Fig. 3d-f. The evolution is carried out in four main steps. Step 1: with CL fixed, the droplet is evolved to reach the target volume. Step 2: the CL is released, and the droplet is evolved further with the CL approaching its final length. Step 3: the mesh near the CL is refined further, which allows small surface curvatures near the fiber to be resolved (Fig. 3f). Step 4: The droplet shape is evolved until L_w changes less than 10 nm between iterations. The final L_w is measured as the horizontal distance between the furthest points defining the CL.

The SE simulation solves L_w as a function of θ_c and the other geometrical parameters:

$$L_w = f^{-1}(\theta_c; h, V, r_f), \quad (4)$$

which is the inverse function of (2). To find the θ_c that results in the L_w measured with machine vision, we employ the method of successive linear interpolation, based on two initial guesses. However, this method requires several simulations for each side-view frame to approximate L_w with low uncertainty. This may result in an impractical computational time to simulate all frames of an experiment (~ 3000 frames @ 100 fps).

To circumvent the computational overhead associated with solving the inverse function (4) for a large number of points, we employ a curve-fitting strategy. The fiber radius is constant during each experiment, and we set the volume of the droplet

to the mean volume, i.e., $(V_i + V_f)/2$, leaving L_w and h as free parameters. A representative subset of 100 simulations is carried out (10 values of θ_c by 10 values of h) and the resulting L_w values are recorded (blue points in Fig. 3g). A 4th order polynomial is fit to the data points (the fitting plane in Fig. 3g). Typical values for the standard deviation of the residuals of the fit range between 0.12° and 0.27° . Some simulations fail to converge and are excluded from the dataset.

Using the fitted function, we can easily calculate θ_c on all frames of an approach-retract measurement. Fig. 3h shows an example a θ_c versus L_w curve obtained for an approach-retract measurement. The information provided by the curve is similar to the θ_c versus baseline diameter curves obtained in convectional contact angle goniometry [25], from which advancing and receding contact angles can be measured. The measurement starts after the droplet contacts the fiber and stabilizes (also known as Snap-in event). During the approach phase (blue segment of the curve in Fig. 3h) the wetting length grows as the fiber is pressed against the droplet. During the retraction phase (red segment) L_w is approximately constant at first, near $675 \mu\text{m}$. Then L_w recedes with approximately constant θ_c . The measurement ends when the droplet detaches from the fiber (also known as Pull-off). The shaded blue and red regions are used to calculate the advancing and receding angles $\theta_a = 89 \pm 1.0^\circ$, $\theta_r = 73.7 \pm 0.4^\circ$, respectively, where the uncertainty represents the standard deviation.

As mentioned, the data used to produce the fitted function assumes a constant droplet volume, however, during a ~ 30 s experiment the droplet evaporates around 2.8 %, which may cause a discrepancy in the curve of Fig. 3h. To verify the accuracy of the fitted function we simulate two points during the approach phase and two points during the retraction phase (green points in Fig. 3h), using the successive linear interpolation method. A maximum discrepancy of 0.28° is observed between the fitted model and the direct simulation points, which is within the uncertainty range of the fitted function.

The sensitivity of the method can be estimated by taking the partial derivative of the fitted function with respect to L_w , $|\partial\theta_c/\partial L_w|$. We find the sensitivity of the method is at most $0.25^\circ/\mu\text{m}$, i.e., for an error of $1 \mu\text{m}$ (~ 1 pixel) in the estimation of L_w , the resulting contact angle will vary only 0.25° .

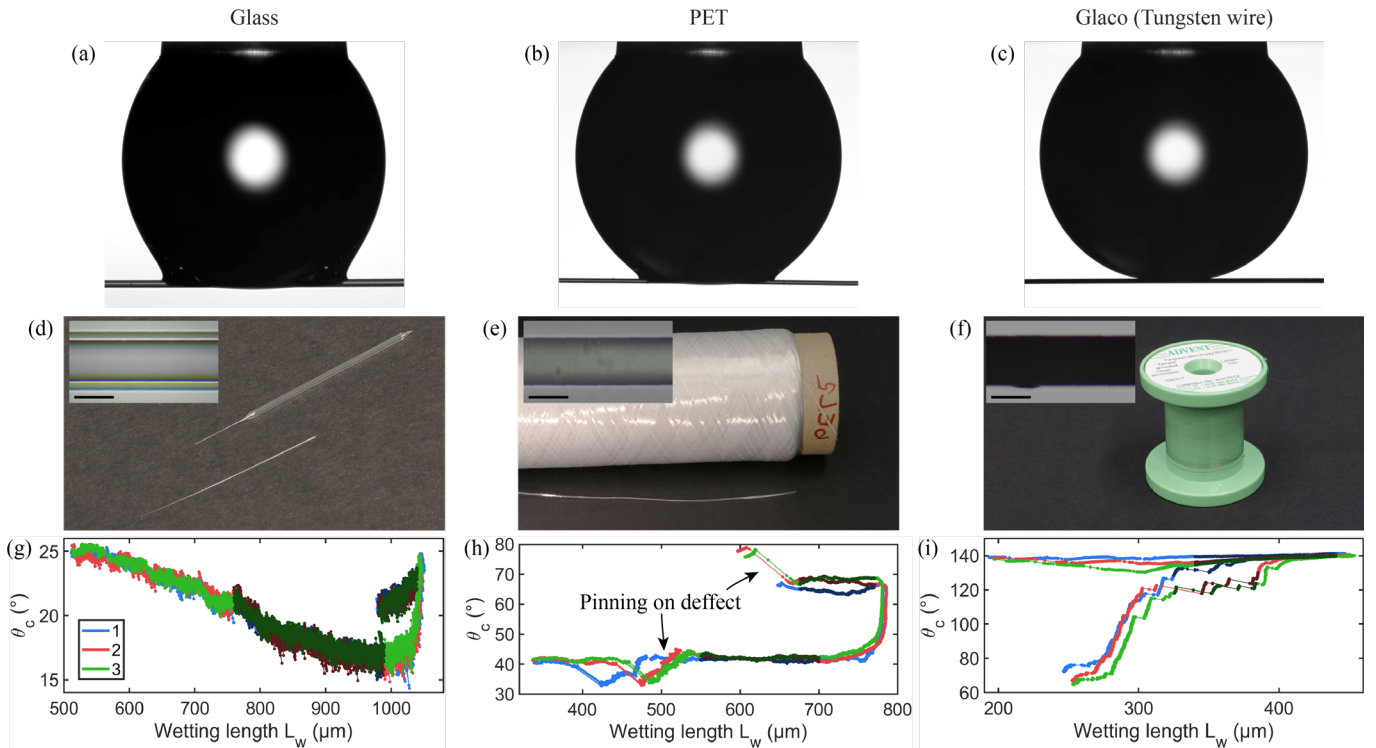


Figure 4 – Results from measurements of three different types of fibers. (a-c) Side-view image during the approach phase at same droplet height h . (d) Two pieces of the glass capillary resulting from the glass pulling process. Bottom piece corresponds to the segment used for wetting characterization. Inset shows micrograph of the fiber (Inset scale bar: 20 μm). (e) Spool of PET fibers. Inset shows micrograph of the fiber (Inset scale bar: 20 μm). (f) Spool of uncoated tungsten wire. Inset shows micrograph of the coated fiber (Inset scale bar: 20 μm). (g-i) Three consecutive measurements of contact angle θ_c versus wetting length L_w obtained on each fiber. Blue, red and green are first, second and third measurements, respectively. The shaded segments on each curve mark the regions manually selected to calculate advancing and receding angles (See Fig. 3h for details).

VI. RESULTS

We applied our method to three types of fibers, presented in Fig. 4, one commercially available soft textile fiber, PET ($r_f = 12.1 \mu\text{m}$), and two rigid fibers, a borosilicate glass capillary ($r_f = 21.0 \mu\text{m}$), and a tungsten wire coated with a commercial hydrophobic coating (Glaco, $r_f = 12.6 \mu\text{m}$, see Appendix I for sample preparation methods). Side-view images during acquisition are shown in Fig. 4a-c and microscope images of each fiber are presented in Fig. 4d-f. Three consecutive approach-retract measurements were made for each fiber. The side-view images were analyzed to obtain the wetting length and disk-to-fiber height, from which simulations were made and the respective fitting models were created. The resulting contact angles versus wetting length are presented in Fig. 4g-i. The mean advancing and receding contact angles are shown in Table I.

Comparison with literature can be challenging due to differences in material properties, sample preparation conditions, and the measurement method used. The PET fiber presents contact angles on the lower end of what is typically shown in literature, between 66° to 91° in [26] and 75° in [27] for flat PET surfaces, yet plausible for this material.

The glass fiber results show contact angle values below 25° , in agreement with the literature for water-rinsed glass (Table 2 of [28]). The wetting properties of glass materials are typically superhydrophilic ($\theta_c < 10^\circ$), and the actual contact angle depends on surface preparation conditions, where contamination leads to higher values. However, it should be

noted that for $\theta_c \lesssim 40^\circ$ the droplet may wet the underside of the fiber, resulting in a different droplet-fiber conformation, which our simulations do not describe well. For this reason, even though the fitted function extends into low contact angles, the accuracy of the measurement requires further investigation.

The Glaco-coated tungsten wire presents hydrophobic wetting properties. These values are however still low when compared with the literature ($\theta_a = 170^\circ$ and $\theta_r = 163^\circ$ in [21]). The low advancing angle can be explained by the underestimation of the wetting length measured from our image analysis algorithm during the approach phase. This is due to the droplet occluding the region near the fiber at such high θ_c . On the other hand, determining the receding contact angle is more challenging due to the unusual wetting behavior observed in Glaco-coated wire, where the droplet depins in successive events, as seen in Fig. 4i.

The measurement of the PET fiber, Fig. 4h, also shows the impact of a small fiber imperfection present on the right-hand side of the fiber. While advancing, the right side of the CL remained pinned at the imperfection, making the droplet shape asymmetric between the left and right sides skewing the contact angle results. After the fiber was pressed on the droplet enough, the defect was overcome. The regions of the curve used to calculate θ_a and θ_r were selected to avoid the sections of the curve affected by the imperfection.

VII. CONCLUSION

This work presents a novel method for characterizing advancing and receding contact angles of soft and rigid fibers. The probe consists of a droplet attached to a disk, which allows great stability of the droplet during each experiment, enabling advancing and receding contact angles to be calculated across a wide range of contact angles. The experiments are carried out with a conventional side-view camera and precision motorized stages, which, combined with precise volume control, allow great repeatability. The side-view images also provide

TABLE I – ADV. AND REC. CONTACT ANGLES ON DIFFERENT FIBERS

Fiber type	θ_a ($^\circ$)	θ_r ($^\circ$)
PET	66.8 ± 0.6	41.9 ± 0.5
Glass	21.6 ± 0.9	18.2 ± 1.3
Glaco (Tungsten wire)	138.8 ± 1.1	126.1 ± 2.5

qualitative information on the wetting phenomena, which significantly helps interpret the resulting data.

The three different types of fibers characterized showcase the wide range of contact angles the method can be applied. The great sensitivity and repeatability of our method may open new doors for the scientific study of the wetting properties of single fibers. Future work for our method could include improvements to the simulation and modelling, such as accounting for tilt and curvature of the fiber in simulation; validation of the method with fibers of known wetting properties, where results can be compared to flat samples of the same material and processing; and better estimation of L_w in the superhydrophobic regime, which could be achieved by customizing the threshold used in the image analysis (Fig. 2f) to different droplet conformation.

APPENDIX I – SAMPLE PREPARATION

The glass capillary was produced from a 1 mm diameter borosilicate capillary (World Precision Instruments, mode no. 1B100-6) pulled with a micro-needle glass puller (model PN-31, Narishige Japan). A tungsten wire (W5573, Advent Research) with a nominal diameter of 25 μm was coated with Glaco Mirror Coat Zero spray (Soft99 Co.).

The PET fiber (Virgin 3.3 dtex PET filaments, Swerea IVF, Sweden) and Glaco-coated tungsten wire were mounted on a glass holder using double-sided tape with a free-hanging length of 10 mm. Glass pieces were cut using a Disco DAD3220 dicing machine from microscope slides (VWR 631-1550). To prevent fiber bending during characterization, a preload was applied to the soft PET fiber before taping (500 mg weight). The glass fiber was mounted on a custom plastic holder with the ends fixed in place with UV curing glue (Delo GB310), with a free hanging length of 20 mm. The radius of each fiber was measured with an optical microscope, model Axioscope 5, Zeiss.

ACKNOWLEDGMENTS

The research was supported by multi-disciplinary doctoral study funding from Aalto Doctoral School of Electrical Engineering, the Academy of Finland (#331149) and Academy of Finland Center of Excellence Program (2022-2029) in Life-Inspired Hybrid Materials (LIBER) (#346109).

REFERENCES

- [1] F. Geyer *et al.*, “When and how self-cleaning of superhydrophobic surfaces works,” *Sci Adv*, vol. 6, no. 3, Jan. 2020, doi: 10.1126/sciadv.aaw9727.
- [2] D. Nioras, K. Ellinas, V. Constantoudis, and E. Gogolides, “How Different Are Fog Collection and Dew Water Harvesting on Surfaces with Different Wetting Behaviors?,” *ACS Appl Mater Interfaces*, vol. 13, no. 40, pp. 48322–48332, Oct. 2021, doi: 10.1021/acsami.1c16609.
- [3] V. Flauraud *et al.*, “Nanoscale topographical control of capillary assembly of nanoparticles,” *Nat Nanotechnol*, vol. 12, no. 1, pp. 73–80, Jan. 2017, doi: 10.1038/nnano.2016.179.
- [4] A. E. Ellakwa, A. C. Shortall, and P. M. Marquis, “Influence of fiber type and wetting agent on the flexural properties of an indirect fiber reinforced composite,” *J Prosthet Dent*, vol. 88, no. 5, pp. 485–490, Nov. 2002, doi: 10.1067/mp.2002.129303.
- [5] T. Xu, Y. Lin, M. Zhang, W. Shi, and Y. Zheng, “High-Efficiency Fog Collector: Water Unidirectional Transport on Heterogeneous Rough Conical Wires,” *ACS Nano*, vol. 10, no. 12, pp. 10681–10688, Dec. 2016, doi: 10.1021/acs.nano.6b05595.
- [6] A. Tuteja *et al.*, “Designing Superoleophobic Surfaces,” *Science* (1979), vol. 318, no. 5856, pp. 1618–1622, Dec. 2007, doi: 10.1126/science.1148326.
- [7] B. Chang, Y. H. Feng, J. L. Jin, and Q. Zhou, “Ejected Droplet-Directed Transportation and Self-Alignment of Microfibers to Micro Trenches,” *Journal of Microelectromechanical Systems*, vol. 30, no. 5, pp. 751–758, Oct. 2021, doi: 10.1109/JMEMS.2021.3099374.
- [8] Bihai Song, Alexander Bismarck, and Jürgen Springer, “Contact Angle Measurements on Fibers and Fiber Assemblies, Bundles, Fabrics, and Textiles,” in *Surface and Interfacial Tension*, S. Hartland, Ed., Zurich, 2004.
- [9] M. M. Amrei, M. Davoudi, G. G. Chase, and H. V. Tafreshi, “Effects of roughness on droplet apparent contact angles on a fiber,” *Sep Purif Technol*, vol. 180, pp. 107–113, Jun. 2017, doi: 10.1016/j.seppur.2017.02.049.
- [10] B. J. Carroll, “The accurate measurement of contact angle, phase contact areas, drop volume, and Laplace excess pressure in drop-on-fiber systems,” *J Colloid Interface Sci*, vol. 57, no. 3, pp. 488–495, Dec. 1976, doi: 10.1016/0021-9797(76)90227-7.
- [11] J.-I. Yamaki and Y. Katayama, “New method of determining contact angle between monofilament and liquid,” *J Appl Polym Sci*, vol. 19, no. 10, pp. 2897–2909, Oct. 1975, doi: 10.1002/app.1975.070191025.
- [12] G. McHale and M. I. Newton, “Global geometry and the equilibrium shapes of liquid drops on fibers,” *Colloids Surf A Physicochem Eng Asp*, vol. 206, no. 1–3, pp. 79–86, Jul. 2002, doi: 10.1016/S0927-7757(02)00081-X.
- [13] B. J. Carroll, “Equilibrium conformations of liquid drops on thin cylinders under forces of capillarity. A theory for the roll-up process,” *Langmuir*, vol. 2, no. 2, pp. 248–250, Mar. 1986, doi: 10.1021/la00068a024.
- [14] T. Bohners, “The Do’s and Don’ts of Wettability Characterization in Textiles,” *J Adhes Sci Technol*, vol. 25, no. 16, pp. 2005–2021, Jan. 2011, doi: 10.1163/016942410X544811.
- [15] T. Bohners and J. S. Gutmann, “Procedures for the Characterization of Wettability and Surface Free Energy of Textiles - Use, Abuse, Misuse and Proper Use,” in *Progress in Adhesion and Adhesives*, Wiley, 2020, pp. 259–293. doi: 10.1002/9781119749882.ch9.
- [16] C. Della Volpe, L. Fambri, S. Siboni, and M. Brugnara, “Wettability of Porous Materials III: Is the Wilhelmy Method Useful for Fabrics Analysis?,” *J Adhes Sci Technol*, vol. 24, no. 1, pp. 149–169, Jan. 2010, doi: 10.1163/016942409X12538812516274.
- [17] N. M. Farhan, H. Aziz, and H. V. Tafreshi, “Simple method for measuring intrinsic contact angle of a fiber with liquids,” *Exp Fluids*, vol. 60, no. 5, p. 87, May 2019, doi: 10.1007/s00348-019-2733-2.
- [18] S. L. Schellbach, S. N. Monteiro, and J. W. Drelich, “A novel method for contact angle measurements on natural fibers,” *Mater Lett*, vol. 164, pp. 599–604, Feb. 2016, doi: 10.1016/j.matlet.2015.11.039.
- [19] M. Jamali and H. V. Tafreshi, “Studying droplet adhesion to fibers using the magnetic field: a review paper,” *Exp Fluids*, vol. 62, no. 8, p. 161, Aug. 2021, doi: 10.1007/s00348-021-03258-9.
- [20] T. Huhtamäki, X. Tian, J. T. Korhonen, and R. H. A. Ras, “Surface-wetting characterization using contact-angle measurements,” *Nat Protoc*, vol. 13, no. 7, pp. 1521–1538, Jul. 2018, doi: 10.1038/s41596-018-0003-z.
- [21] V. Liimatainen *et al.*, “Mapping microscale wetting variations on biological and synthetic water-repellent surfaces,” *Nat Commun*, vol. 8, no. 1, pp. 1–7, 2017, doi: 10.1038/s41467-017-01510-7.
- [22] A. Vieira, W. Cui, V. Jokinen, R. H. A. Ras, and Q. Zhou, “Through-drop imaging of moving contact lines and contact areas on opaque water-repellent surfaces,” *Soft Matter*, 2023, doi: 10.1039/D2SM01622B.
- [23] J. P. Lewis, “Fast Normalized Cross-Correlation,” *Ind. Light Magic*, vol. 10, Jun. 2001.
- [24] K. A. Brakke, “The Surface Evolver,” *Exp Math*, vol. 1, no. 2, pp. 141–165, Jan. 1992, doi: 10.1080/10586458.1992.10504253.
- [25] Biolin Scientific, “Dynamic Contact Angle,” <https://www.biolinscientific.com/measurements/dynamic-contact-angle#how-is-dynamic-contact-angle-measured>, Aug. 03, 2023.
- [26] T. Homola, L. Y. L. Wu, and M. Černák, “Atmospheric Plasma Surface Activation of Poly(Ethylene Terephthalate) Film for Roll-To-Roll Application of Transparent Conductive Coating,” *J Adhes*, vol. 90, no. 4, pp. 296–309, Apr. 2014, doi: 10.1080/00218464.2013.794110.
- [27] S. Jasmee, G. Omar, N. A. B. Masripan, A. A. Kamarolzaman, A. S. Ashikin, and F. Che Ani, “Hydrophobicity performance of polyethylene terephthalate (PET) and thermoplastic polyurethane (TPU) with thermal effect,” *Mater Res Express*, vol. 5, no. 9, p. 096304, Aug. 2018, doi: 10.1088/2053-1591/aad81e.
- [28] A. L. Sumner *et al.*, “The nature of water on surfaces of laboratory systems and implications for heterogeneous chemistry in the troposphere,” *Physical Chemistry Chemical Physics*, vol. 6, no. 3, p. 604, 2004, doi: 10.1039/b308125g.